BI-DIRECTIONAL LIGHT TRANSMISSION PROPERTIES ASSESSMENT FOR VENETIAN BLINDS: COMPUTER SIMULATIONS COMPARED TO PHOTOGONIOMETER MEASUREMENTS

Marilyne Andersen and Jean-Louis Scartezzini
Solar Energy and Building Physics Laboratory (LESO-PB), Swiss Federal Institute of Technology (EPFL), Bâtiment LE, Lausanne 1015, Switzerland, tel: +41 21 693 45 51, fax: +41 21 693 27 22, e-mail: marilyne.andersen@epfl.ch

Michael D. Rubin and Rebecca C. Powles
Lawrence Berkeley National Laboratory (LBNL), University of California, 1 Cyclotron Road, MS 2-300, Berkeley CA 94720-8134, USA

Abstract – An accurate evaluation of daylight distribution through advanced fenestration systems (complex glazing, solar shading systems) requires the knowledge of their Bi-directional light Transmission Distribution Function (BTDF). An innovative equipment for the experimental assessment of these bi-directional functions has been developed, based on a digital imaging detection system. An extensive set of BTDF measurements was performed with this photogoniometer on venetian blinds presenting curved slats with a mirror coating on the upper side. In this paper, the measured data are compared with ray-tracing results achieved with a virtual copy of the device, that was constructed with a commercial ray-tracing software. The model of the blind was created by implementing the measured reflection properties of the slats coatings in the ray-tracing calculations. These comparisons represent an original and objective validation methodology for detailed bi-directional properties for a complex system; the good agreement between the two methods, yet presenting very different parameters and assessment methodologies, places reliance both on the digital-imaging detection system and calibration, and on the potentiality of a flexible calculation method combining ray-tracing simulations with simple components measurements.

1. INTRODUCTION

To optimize the use and design of advanced fenestration systems, and thus efficiently control solar gain and daylighting through windows, there is a need for detailed knowledge of their optical properties. As their variation with the angle of incidence often proves to be critical, such properties should be assessed taking both the incident and emerging directions into account, i.e. according to bidirectional measurements (BTDFs, BRDFs), that are performed with a photogoniometer.

As shown by the work presented in Andersen et al. (2003), the validation of these data lacks absolute standards on full-scale systems, and ray-tracing calculations thus provide a useful and objective point of comparison for validating BT(R)DF data in a roundabout approach. Furthermore, computational methods prove to be a valuable tool for parametric studies, and their combination with experimental methods, restricting the latter to the optical properties assessment of unknown coatings or materials only, will greatly increase flexibility and efficiency.

Comparisons between different assessment methods for the optical performances of glazing or shading systems have been realized in various ways, such as: to test a new ray-tracing approach for thermal radiation assessment (Campbell, 1998) or prismatic panels performances (Compagnon, 1994); to determine the daylight distribution inside a room and compare RADIANCE calculations with test office measurements (Reinhart and Walkenhorst, 2001); for developing an angle-dependent Solar Heat Gain Coefficient evaluation procedure and comparing measurements either to ray-tracing results obtained with the software OptiCAD® (Kuhn et al., 2001) or to matrix layer calculations (Klems et al., 1997); to compare photogoniometric data with results provided by an analytic model (Breitenbach et al., 2001; Rosenfeld, 1996).

However, the quantity considered for these comparative studies remained the directional-hemispherical transmittance, which represents the global light transmittance, and as such integrates the associated bidirectional function over the emerging space. Andersen et al. (2003) thus appears as a first attempt to validate detailed experimental BTDF data for an advanced glazing system, namely prismatic panels, by comparing them to ray-tracing calculation results. This paper goes further in this prospect, by choosing a venetian blind as study case, and consequently increasing the model complexity, as it presents geometric and coating properties less easily modeled than an acrylic prism with macroscopic grating.

Experimental conditions for BTDF characterization were here reproduced virtually with the commercial forward ray-tracer TRACEPRO®[1] for a venetian blind prototype manufactured by Baumann-Hüppe AG. This blind presents curved slats with a mirror coating on the upper side, characteristics that were precisely measured and implemented in the model. Computer simulation results were then compared to measured BTDF data, that were assessed with the digital imaging-based photogoniometer developed at the Swiss Federal Institute of Technology (EPFL) (Andersen et al., 2001; Andersen, 2002).

[1] TRACEPRO®, v. 2.3 & 2.4, Lambda Research Corporation.

2. CHARACTERISTICS AND MODELING OF VENETIAN BLINDS

The venetian blind considered in this study is shown on Figure 1. As detailed in section 2.2, the mirror coating makes the upper slat side a very specular surface, whereas the beige paint presents diffuse properties, close to lambertian. These features increase the interest of analyzing such a system, as the numerous inter-reflections undergone by the incident light rays consist of a combination of very different reflection types.

Figure 1: Venetian blind prototype presenting curved slats with mirror and diffuse beige coatings on their upper and lower faces respectively.

This venetian blind's BTDF was determined experimentally for a set of 23 different incident directions for two slats arrangements, horizontal (0° tilt) and oblique (45° tilt), amongst which 10 were selected for comparisons to simulations for the 0° slats and 5 for the 45° slats, as explained in section 4.

Before modeling a system with a ray-tracing tool, its geometric and coating characteristics have to be precisely and fully known, in order to be implemented properly in the model.

2.1 Geometric properties

The slat's geometric properties were determined with micrometric measurement tools. The obtained dimensions are given in Figure 2; the curving radius R, deduced from equation (1), is equal to 96.9 mm.

Through a combination of subtractions and intersections of primitive solids (Fig. 4(a)), a virtual element presenting the same features was created in TRACEPRO®, and its edges were thereafter rounded to avoid aberrant ray paths.

$$R = \frac{(e-\varepsilon)^2 + \frac{(L-\frac{\varepsilon L}{2R+\varepsilon})^2}{4}}{2(e-\varepsilon)} \qquad (1)$$

An arrangement of 7 of these individual slats was then created according to the measured positions of the physical ones on the sample holder; as far as the modeling of the 45° tilt configuration is concerned, the slats rotation axes were defined taking the dimensions of the mechanical revolving system into account. The obtained venetian blind model is represented on Figure 4(b) for this configuration.

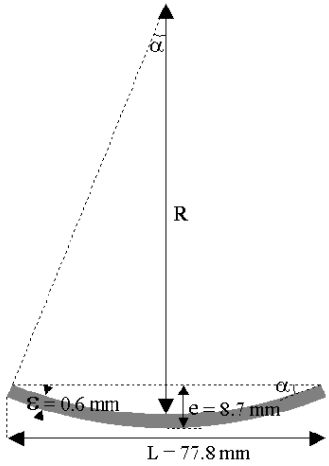

Figure 2: Geometric properties of individual venetian blind slat.

2.2 Mirror and paint coatings

The assessment of the reflective properties of the slats paint and mirror coatings was achieved at LBNL using the Perkin-Elmer Lambda 19 spectrophotometer with an integrating sphere accessory. The reflectance was measured every 5 nm between 300 and 2500 nm on both sides, and the obtained spectra were corrected with the known reflectance of a calibrated diffuse reflectance standard made of Spectralon. Photopic averages were then taken using the D65 source and CIE 1931 2-degrees observer functions (CIE, 1932); the resulting visible (photopic) total reflectances were 28.6% and 83.7% for the paint and mirror surfaces respectively.

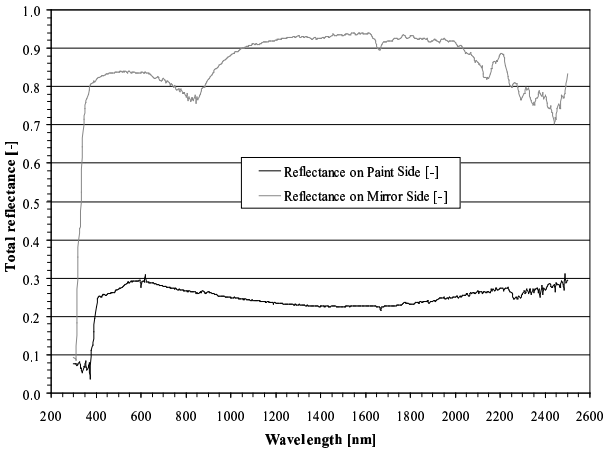

Figure 3: Total reflectances, measured every 5 nm, for both mirror and beige mat paint coatings of the curved venetian blinds slats manufactured by Baumann-Hüppe AG.

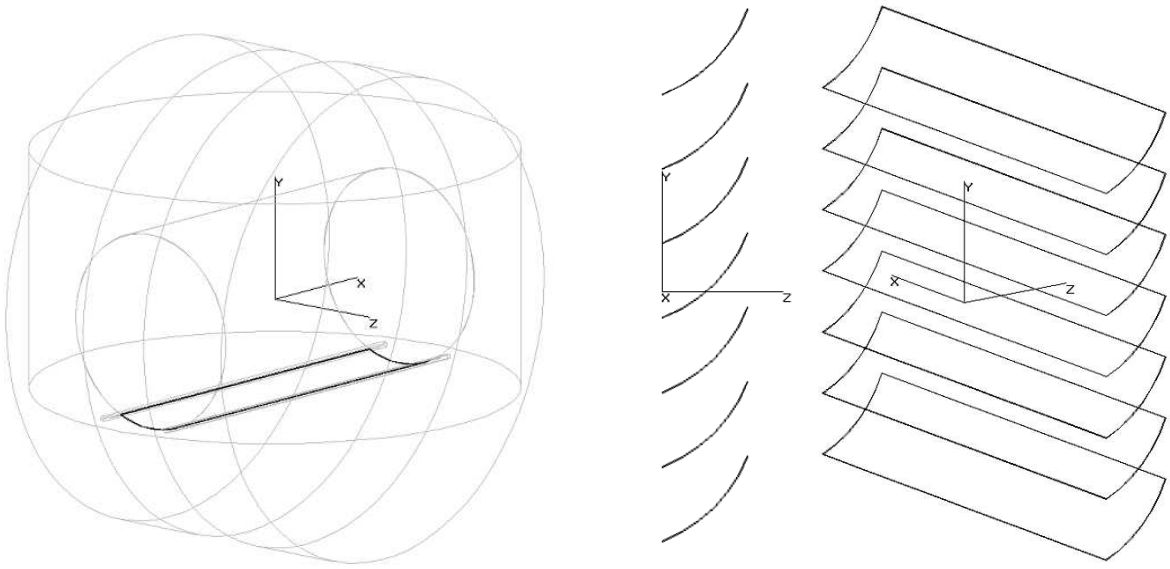

(a) Creation of slat element

(b) 45° tilt slats configuration

Figure 4: Modeling of the venetian blind's geometry.

The obtained spectra are shown on Figure 3 over the complete wavelength interval; their approximation with 50 nm wavelength steps was used for implementing the data into the ray-tracing tool.

For both coatings, the reflectance was measured with and without a light trap to collect the specularly reflected beam. For the paint surface, the scans were almost identical, which means that the reflectance is very diffuse; for the mirror, the scan with light trap was almost zero at all visible wavelengths, showing that it presents highly specular properties. In addition to that, the paint surface value was checked with a different apparatus (Colorimeter CR-200b Minolta for assessing the color coordinates and reflectance of diffuse surfaces) and the results were found to be very close (difference of 3%). When creating the coatings files for TRACEPRO®, only a slight ($\sim$2%) specular component was thus added for the paint surface, and likewise a scattering component for the mirror, otherwise considered respectively perfectly lambertian and specular.

3. VIRTUAL PHOTOGONIOMETER COPY

The experimental assessment method can be found in Andersen et al. (2001): the light transmitted from the sample is reflected by a diffusing triangular panel towards a calibrated Charge-Coupled Device (CCD) camera, used as a multiple-points luminance-meter, which provides a picture of the whole screen; after six 60° rotations of the screen-camera system (with image capture, calibration and processing at each position), the transmitted light distribution is fully known.

To reproduce these assessment conditions virtually, a copy of the photogoniometer was modeled, of same characteristics as the one presented in Andersen et al. (2003) (light source, detection system), except for the following features:

- the discretization grid for BTDF averaging here corresponded to an output resolution ($\Delta\theta_2$, $\Delta\phi_2$) = (10°, 15°), in order to fit the one adopted for the measurements, θ_2 and ϕ_2 being the polar coordinates [°] of the emerging (transmitted) light flux, based on a referential linked to the sample; the detection screens models have thus been altered accordingly, as illustrated in Figure 5(a)
- the sample diaphragm diameter was set to 15 cm, also to be coherent with the experimental situation
- as the rays undergo diffuse reflectances, the flux threshold was lowered to 0.001 in order to keep sufficient track of the scattered rays for a reliable BTDF estimation.

The observed quantity in simulation being the total photometric flux received by each detection zone on the projection screens, the corresponding BTDF values are calculated through equation (2) (Andersen et al., 2003):

$$BTDF(\theta_1, \phi_1, \theta_2, \phi_2) = \frac{\Phi_{2norm}}{\Delta\theta_2 \Delta\phi_2 \sin\theta_2 \cos\theta_2} \qquad (2)$$

where θ_1 and ϕ_1 are the polar coordinates [°] of the incoming light flux and where Φ_{2norm} is the transmitted light flux normalized to the incoming flux; the BTDF averaging intervals $\Delta\theta_2$ and $\Delta\phi_2$ are here expressed in radians.

A ray-tracing plot example is displayed on Figure 5(b) for the 0° slats tilt configuration, under an incident direction (θ_1, ϕ_1) = (12°, 90°). Only a few (about a thousand) of the 200,000 traced rays are shown on the plot, to get a still readable transmitted light distribution.

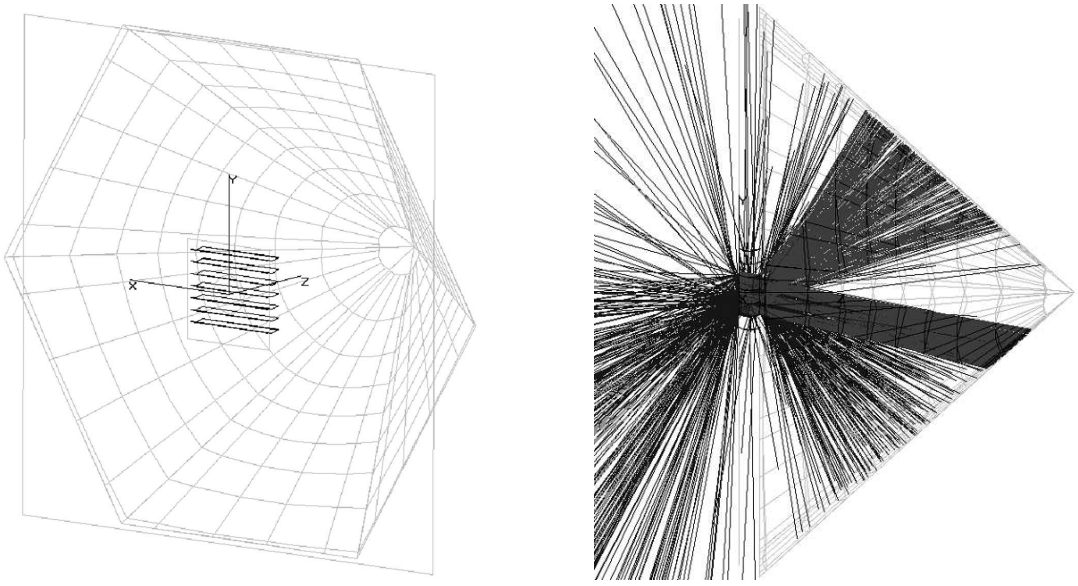

(a) Simulation model for the venetian blind performances assessment: the six absorbing detection screens are split into angular zones of spread ($\Delta\theta_2$, $\Delta\phi_2$) = (10°, 15°)

(b) Traced rays for the 0° tilt configuration, under incidence (θ_1, ϕ_1)=(12°, 90°)

Figure 5: Photogoniometer model for assessing BTDFs with ray-tracing calculations.

4. RESULTS COMPARISON

Once converted into the corresponding BTDF values through equation (2), the simulated fluxes detected in each discretization zone data can be compared to the experimental BTDF values. Both measured and calculated BTDFs being assessed inside given angular areas around the associated couples (θ_2, ϕ_2), they depend on the discretization grid intervals $\Delta\theta_2$ and $\Delta\phi_2$. Indeed, they represent average values of BTDFs inside these areas, and provide a continuous - thus complete - investigation of the transmitted light distribution, unlike point-per-point data that provide BTDF values along specific directions (θ_2, ϕ_2).

In order to point out differences between real and virtual values with high accuracy, two-dimensional plots for varying altitudes ϕ_2 and along given azimuths θ_2 are chosen instead of the more intuitive but less detailed 3D representations in spherical coordinates that are usually adopted for BTDF visualization (Andersen, 2002). The results are shown on Figures 6 and 7; as mentioned in section 3, the grids for BTDF averaging fitted (10°, 15°) intervals.

For each analyzed situation, the relevant outgoing azimuthal planes (i.e. the angles ϕ_2 for which the transmission is non-zero) were determined. Both measured and calculated BTDF data were reported along these outgoing planes as functions of altitude θ_2 for the 15 selected incident directions. For the 0° slats tilt configuration, these incident directions were (0°, 0°), (12°, 90°), (60°, 90°), (20°, 270°), (40°, 270°), (53°, 1°), (31°, 30°), (17°, 45°), (68°, 45°) and (72°, 61°). For the 45° slats tilt, the incident directions were (0°, 0°), (12°, 90°), (20°, 270°), (17°, 45°) and (50°, 315°). The azimuthal planes next to the most relevant ones were also checked (planes $\phi_{2m} \pm \Delta\phi_2$ and $\phi_{2m} \pm 2\Delta\phi_2$, where ϕ_{2m} is the azimuth angle for which the BTDF reaches an extremum value) and generally reveal the same kinds of behaviours as the main plane (but with lower values), as shown on Figures 6(c), 6(f) and 7(c) for instance.

Globally speaking, the obtained results reveal that a remarkable agreement between real and virtual BTDF values is achieved: the observed differences are almost always comprised within the error bars (their determination is explained in section 5) and remain below 8% on average, in relative terms. Even though the transmission features are generally sharp (high gradients increase the risk of having significant dissimilarities between two assessment methods), low discrepancies and an analogous qualitative light behaviour are observed for the experimental and computational methods, as well for the light transmitted directly (rays passing between the slats) as for the light that was redirected after reflection on the curved slats surfaces.

The few situations where the observed discrepancies are higher (as e.g. in Figures 7(a), 7(d) and especially 6(d)) are generally associated to lower BTDF values, where the sensitivity to the simulation conditions is greatly enhanced. If we consider the results of Figure 6(d) in particular, we can observe that they correspond to a light distribution situation where practically all the transmitted rays have undergone a reflection on the paint side of the slats (diffuse surface), which explains why the transmission is so low (global (direct-hemispherical) transmittance of 3%; this value was the same whether assessed with the calculation

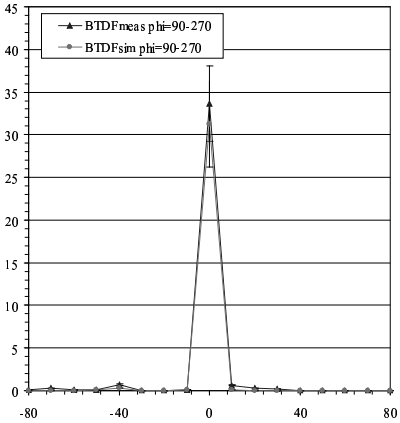

(a) Incidence (θ_1, ϕ_1) = (0°, 0°): Direct transmission peak

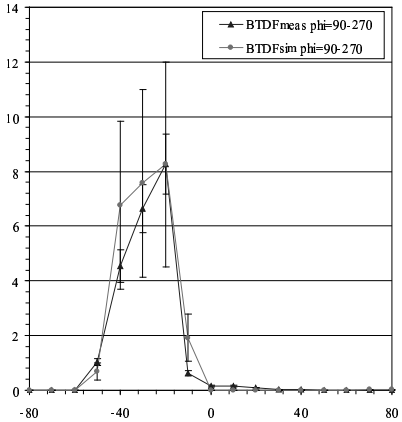

(b) Incidence (θ_1, ϕ_1) = (60°, 90°): Main section view for mirror reflected transmission

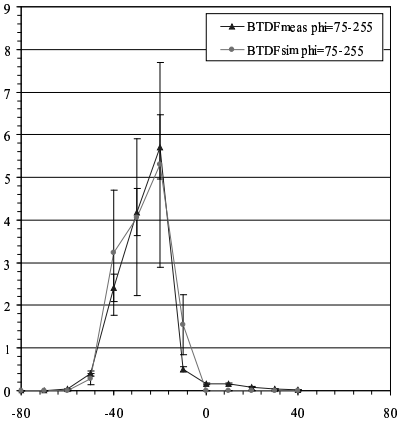

(c) Incidence (θ_1, ϕ_1) = (60°, 90°): Adjacent section view for mirror reflected transmission

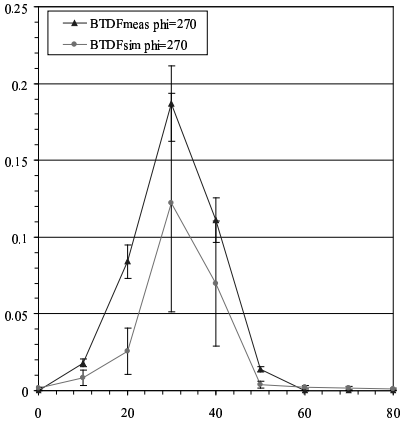

(d) Incidence (θ_1, ϕ_1) = (40°, 270°): Light transmitted after reflection on the slats paint side only

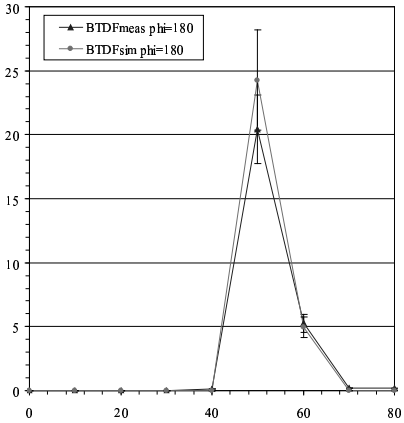

(e) Incidence (θ_1, ϕ_1) = (53°, 1°): Direct transmission peak

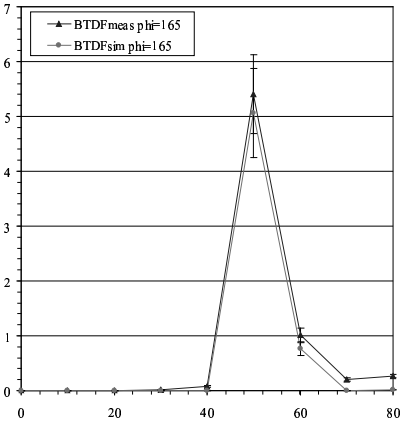

(f) Incidence (θ_1, ϕ_1) = (53°, 1°): Adjacent section view for direct peak

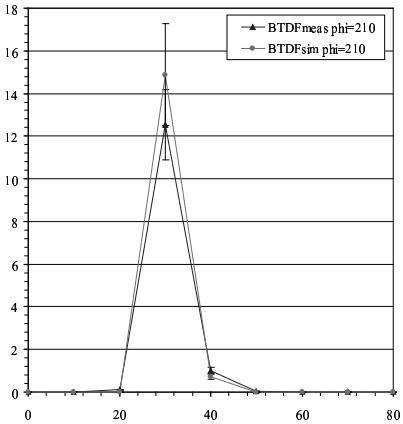

(g) Incidence (θ_1, ϕ_1) = (31°, 30°): Direct transmission peak

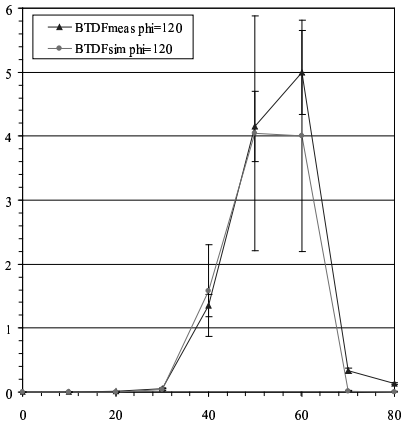

(h) Incidence (θ_1, ϕ_1) = (31°, 30°): Light transmission after reflection on the slats mirror side

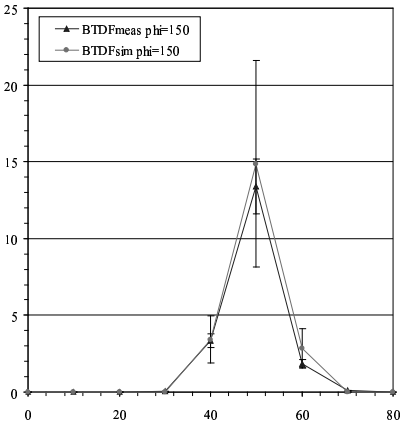

(i) Incidence (θ_1, ϕ_1) = (68°, 45°): Mirror reflected peak

Figure 6: BTDF [sr^{-1}] vs. θ_2 [°] along ϕ_2 planes: comparison of measurements ($BTDF_{meas}$) and calculations ($BTDF_{sim}$) for the 0°slats tilt configuration; for conciseness, some section views show ϕ_2 planes in pairs (90° and 270°, 75° and 255°), the latter being then plotted with negative values for θ_2.

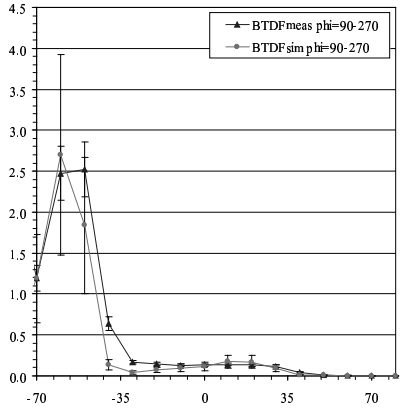

(a) Incidence (θ_1, ϕ_1) = (0°, 0°): Light transmission after reflection on the slats mirror side

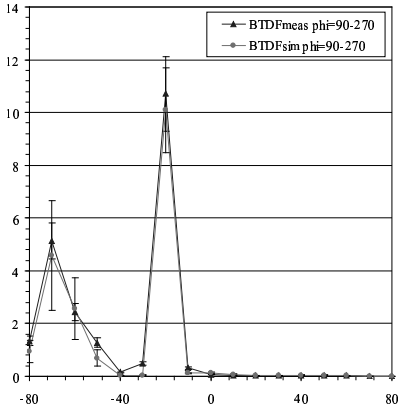

(b) Incidence (θ_1, ϕ_1) = (20°, 270°): Main section view for direct and mirror reflected transmission

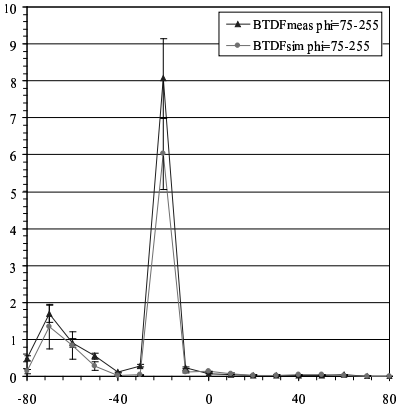

(c) Incidence (θ_1, ϕ_1) = (20°, 270°): Adjacent section view for direct and mirror reflected transmission

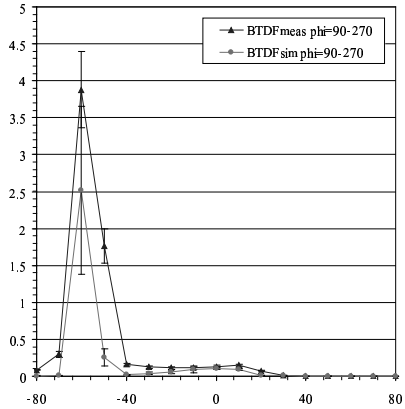

(d) Incidence (θ_1, ϕ_1) = (12°, 90°): Direct and mirror reflected transmission

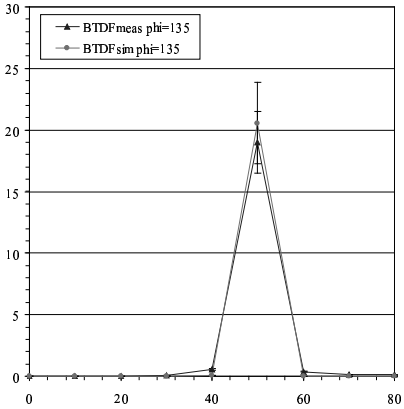

(e) Incidence (θ_1, ϕ_1) = (50°, 315°): Main section view for direct transmission

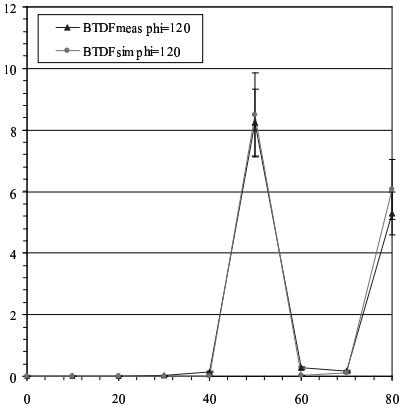

(f) Incidence (θ_1, ϕ_1) = (50°, 315°): Adjacent section view for direct transmission

Figure 7: BTDF [sr^{-1}] vs. θ_2 [°] along ϕ_2 planes: comparison of measurements ($BTDF_{meas}$) and calculations ($BTDF_{sim}$) for the 45°slats tilt configuration; for conciseness, some section views show ϕ_2 planes in pairs (90° and 270°, 75° and 255°), the latter being then plotted with negative values for θ_2.

or the experimental methods) and why it will be considerably influenced by the model parameters, and more specifically by the exact paint coating specular component and reflection coefficient variations over the spectrum.

Figures 6 and 7 therefore make up a positive reciprocal validation, on one hand of the experimental set-up, and more specifically the adopted detection technique and the calibration and correction procedures, and on the other hand of the reliability and applicability of ray-tracing calculations for complex fenestration systems assessment.

5. ERROR ESTIMATION

The relative impact on the BTDF values of the incertitudes due to the CCD camera calibration procedures and other corrections is of 5% (Andersen et al., 2000); the discrepancies connected to the spatial adjustment of the facility components were estimated by modeling slight variations (±0.5°, ±2 mm) in the incident direction or detection screen position and observing the effect on the final results, which was found to be 8%. These considerations therefore lead to a global error of 13% for the measurements, represented by the error bars associated to the "$BTDF_{meas}$" curves in Figures 6 and 7.

As far as the accuracy of the model results is concerned, it was estimated, for the 0° slats configuration, by observing the impact on the final BTDF data of slight modifications of simulation parameters, allowing to appreciate the sensitivity of the results to their exact settings (which can only approximately describe a physical - thus imperfect - venetian blind):

- small difference in the slats tilt (3°anticlockwise when seen from ϕ = 0°, each slat being hence shifted 0.6 mm to keep the interface at the same position)
- half a period slats position shift (37 mm further down)
- variation of the curving radius (±1.8 cm, the slats width being kept)

- neutral mirror coating (constant reflectance of 83.7% over the spectrum, no diffuse component)
- neutral paint coating (constant reflectance of 28.6% over the spectrum, no specular component); this last parameter only affected the results significantly for the incident direction (θ_1, ϕ_1) = (40°, 270°)).

As mentioned in section 2.1, the edges of the venetian blind's slats were rounded in the simulation model, to be as close as possible to the physical prototype and to avoid aberrant ray paths. Nonetheless, sharp edges were proven to be of negligible influence on the BTDF results.

A different numerical model was created for every parameter, only altering the concerned one, and the impact of this modification was evaluated for two different incident directions, - (31°, 30°) and (68°, 45°) -, and all the transmitted directions where the BTDF values were greater than 5% of the curve maximum by determining the resulting variations of the BTDF data, the ones corresponding (mainly) to direct transmission peaks being separated from those corresponding to light transmitted after reflection on the mirror side of the slats. The (40°, 270°) incidence was analyzed apart from the others, in order to assess the effect of the paint coating specifications when the diffuse transmission becomes significant compared to the direct and mirror reflected light.

The relative differences on BTDF results generated by these modifications were averaged, for each studied parameter, over the set of incident and transmitted directions. This lead to incertitude values of about 14%, 5%, 4% and 0.3% for the direct peaks, and 22%, 8%, 33% and 19% for the reflected peaks, respectively associated to the slats tilt angle, position and curving radius, and the mirror coating's specifications; the paint coating parameter's effect was estimated to 58%, which shows how sensitive the results are to even slight model differences when the BTDFs are low.

In the end, global errors of 16%, 45% and 58% were obtained for direct, mirror and paint reflected transmission respectively from calculating the RSS (Root Sum Square) of the relative incertitudes, including the ones due to the limits of the model (threshold ($\sim$1% error), number of emitted rays ($\sim$1%), discretized source spectrum ($\sim$2%): see Andersen et al. (2003). These errors are represented by the error bars associated to the "$BTDF_{sim}$" curves in Figures 6 and 7.

Their large values show that the model's adequacy to provide a perfect copy of the physical blind could rapidly be lowered with a slightly inappropriate choice of simulation parameters, or with flawed or irregularly manufactured slats. However, as shown by the particularly close qualitative but also quantitative agreement between the "$BTDF_{meas}$" and "$BTDF_{sim}$" curves for nearly all the studied situations, the blind's model could here be considered as very satisfactory to conduct a reliable assessment of its transmission performances based on ray-tracing calculations.

6. CONCLUSIONS

The work presented in this paper is a further step in the appraisal of BTDF determination methods, based on comparisons between photogoniometric measurements and ray-tracing simulation results.

In Andersen et al. (2003), prismatic panels of standard refractive indices given by Fresnel laws were chosen to assess this roundabout approach in BTDF validation. Here, more complex systems were chosen, both from the geometrical and the materials points of view: virtual copies of the slats were created taking the dimensions and spatial arrangement of the manufacturer's prototype into account, and the reflective properties of their coatings, mirror on the upper side, beige mat paint on the lower side, were determined experimentally with a spectrophotometer and implemented in the model.

The venetian blind model's transmission performances were then assessed with a virtual copy of the bi-directional photogoniometer developed at the LESO-PB / EPFL: the light source spectrum and beam spread were imitated, and a virtual detection system reproducing the mobile triangular panel used as a projection screen for the transmitted light in the experimental device was modeled. Monte Carlo based ray-tracing calculations were then launched for two slats tilt configurations and 15 different incident directions. The comparisons between simulations and measurements showed remarkably close agreement, with discrepancies in average lower than 8%, despite the very different assessment methods and the important number of parameters that had to be taken into consideration.

This work thus confirms the assertions established in Andersen et al. (2003), that supported the geometrical optics approach's ability to provide BTDF results with a precision sufficient for glazing systems evaluations, and, conversely, that validated the experimental BTDF assessment technique. It even enhances them by showing that they remain valid with more complex systems, where critical components' optical properties have to be determined experimentally beforehand, and implemented in the ray-tracing tool. It is indeed shown that the accuracy reached in such intermediate characterizations is sufficient for final calculation results to be accurate and reliable, and strongly supports the concept of an assessment method combining both experimental and computational aspects.

ACKNOWLEDGEMENTS

This work was supported by the Assistant Secretary for Energy Efficiency and Renewable Energy, Office of Building Technology, State and Community Programs, Office of Building Research and Standards of the U.S. Department of Energy under Contract No. DE-AC03-76SF00098. Marilyne Andersen was supported by a joint funding from the Lawrence Berkeley National Laboratory and the Swiss National Science Foundation, fellowship 81EL-66225.

The authors wish to thank Dr. Laurent Michel for his kind help in determining the blind's geometric properties, as well as Christian Roecker and Pierre Loesch for their contribution in the photogoniometer's mechanical development.

REFERENCES

Andersen, M. (2002). Light distribution through advanced fenestration systems. *Building Research and Information*, 30(4):264–281.

Andersen, M., Michel, L., Roecker, C., and Scartezzini, J.-L. (2001). Experimental assessment of bi-directional transmission distribution functions using digital imaging techniques. *Energy and Buildings*, 33(5):417–431.

Andersen, M., Rubin, M., and Scartezzini, J.-L. (2003). Comparison between ray-tracing simulations and bi-directional transmission measurements on prismatic glazing. *Solar Energy*, 74(2):155–171.

Andersen, M., Scartezzini, J.-L., Roecker, C., and Michel, L. (2000). Bi-directional Photogoniometer for the Assessment of the Luminous Properties of Fenestration Systems. CTI Project 3661.2, LESO-PB/EPFL, Lausanne.

Breitenbach, J., Lart, S., Längle, I., and Rosenfeld, J. (2001). Optical and thermal performance of glazing with integral venetian blinds. *Energy and Buildings*, 33(5):433–442.

Campbell, N. (1998). *A Monte Carlo approach to thermal radiation distribution in the built environment*. PhD. thesis, University of Nottingham, Nottingham.

CIE (1932). *Commission Internationale de l'Eclairage Proceedings, 1931*. Cambridge University Press, Cambridge.

Compagnon, R. (1994). *Simulations numériques de systèmes d'éclairage naturel à pénétration latérale (Numerical simulations of daylighting systems for side-lighting)*. PhD. thesis, Ecole Polytechnique Fédérale de Lausanne, Lausanne.

Klems, J., Warner, J., and Kelley, G. (1997). A comparison between calculated and measured SHGC for complex glazing systems. In *ASHRAE Transactions, Vol. 102(1)*, pages 931–939, Atlanta, Feb. 17-21 (1996).

Kuhn, T., Bühler, C., and Platzer, W. (2001). Evaluation of overheating protection with sun-shading systems. *Solar Energy*, 69(Suppl. 6):59–74.

Reinhart, C. and Walkenhorst, O. (2001). Validation of dynamic RADIANCE-based daylight simulations for a test office with external blinds. *Energy and Buildings*, 33(7):683–697.

Rosenfeld, J. (1996). On the calculation of the total solar energy transmittance of complex glazings. In *Proceedings of the 8th International Meeting on Transparent Insulation*, Freiburg, Germany.